

Theoretical Study of the Mechanism of the Hydride Transfer between Ferredoxin–NADP⁺ Reductase and NADP⁺: The Role of Tyr303

Isaias Lans,[†] Milagros Medina,^{*,†} Edina Rosta,[‡] Gerhard Hummer,[§] Mireia Garcia-Viloca,^{*,||} José M. Lluch,^{||} and Àngels González-Lafont^{||}

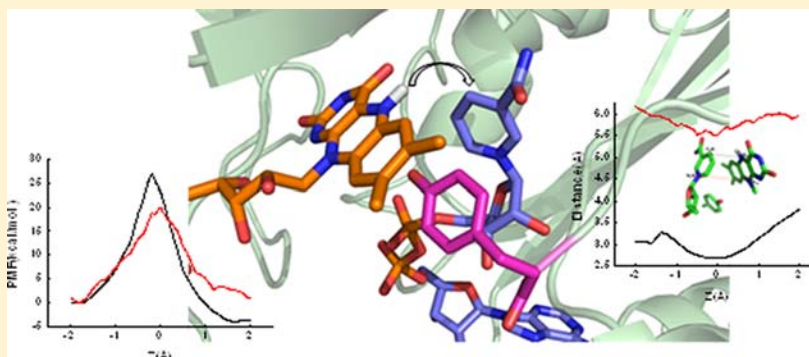
[†]Departamento de Bioquímica y Biología Molecular y Celular, Facultad de Ciencias, and Institute for Biocomputation and Physics of Complex Systems (BIFI)-Joint Unit BIFI-IQFR (CSIC), Universidad de Zaragoza, 50009 Zaragoza, Spain

[‡]Department of Chemistry, King's College London, London SE1 1UL, United Kingdom

[§]Laboratory of Chemical Physics, National Institute of Diabetes and Digestive and Kidney Diseases, National Institutes of Health, Bethesda, Maryland 20892, United States

^{||}Departament de Química and Institut de Biotecnologia i de Biomedicina, Universitat Autònoma de Barcelona, 08193 Bellaterra (Barcelona), Spain

S Supporting Information



ABSTRACT: During photosynthesis, ferredoxin–NADP⁺ reductase (FNR) catalyzes the electron transfer from ferredoxin to NADP⁺ via its FAD cofactor. The final hydride transfer event between FNR and the nucleotide is a reversible process. Two different transient charge-transfer complexes form prior to and upon hydride transfer, FNR_{rd}–NADP⁺ and FNR_{ox}–NADPH, regardless of the hydride transfer direction. Experimental structures of the FNR_{ox}:NADP⁺ interaction have suggested a series of conformational rearrangements that might contribute to attaining the catalytically competent complex, but to date, no direct experimental information about the structure of this complex is available. Recently, a molecular dynamics (MD) theoretical approach was used to provide a putative organization of the active site that might represent a structure close to the transient catalytically competent interaction of *Anabaena* FNR with its coenzyme, NADP⁺. Using this structure, we performed fully microscopic simulations of the hydride transfer processes between *Anabaena* FNR_{rd}/FNR_{ox} and NADP⁺/H, accounting also for the solvation. A dual-level QM/MM hybrid approach was used to describe the potential energy surface of the whole system. MD calculations using the finite-temperature string method combined with the WHAM method provided the potential of mean force for the hydride transfer processes. The results confirmed that the structural model of the reactants evolves to a catalytically competent transition state through very similar free energy barriers for both the forward and reverse reactions, in good agreement with the experimental hydride transfer rate constants reported for this system. This theoretical approach additionally provides subtle structural details of the mechanism in wild-type FNR and provides an explanation why Tyr303 makes possible the photosynthetic reaction, a process that cannot occur when this Tyr is replaced by a Ser.

1. INTRODUCTION

Plastidic ferredoxin–NADP⁺ reductases (FNRs) accept electrons by two sequential one-electron transfer steps from two molecules of the one-electron donor ferredoxin to generate their fully reduced hydroquinone state, FNR_{rd}, through the formation of an intermediate neutral semiquinone form, FNR_{sq}. FNR_{rd} then transfers both electrons as a hydride to the nicotinamide adenine dinucleotide phosphate (NADP⁺) coenzyme in a single step (Figure 1A).^{1,2} FNR folds into two

domains, one of which presents a non-covalently bound flavin adenine dinucleotide (FAD), while the other binds NADP⁺. In *Anabaena* FNR (*AnFNR*), the FAD-binding domain includes residues 1–138. It is made up of six antiparallel β -strands arranged in two perpendicular β -sheets with a short α -helix at the bottom, and another α -helix and a long loop that is

Received: October 19, 2012

Published: November 26, 2012

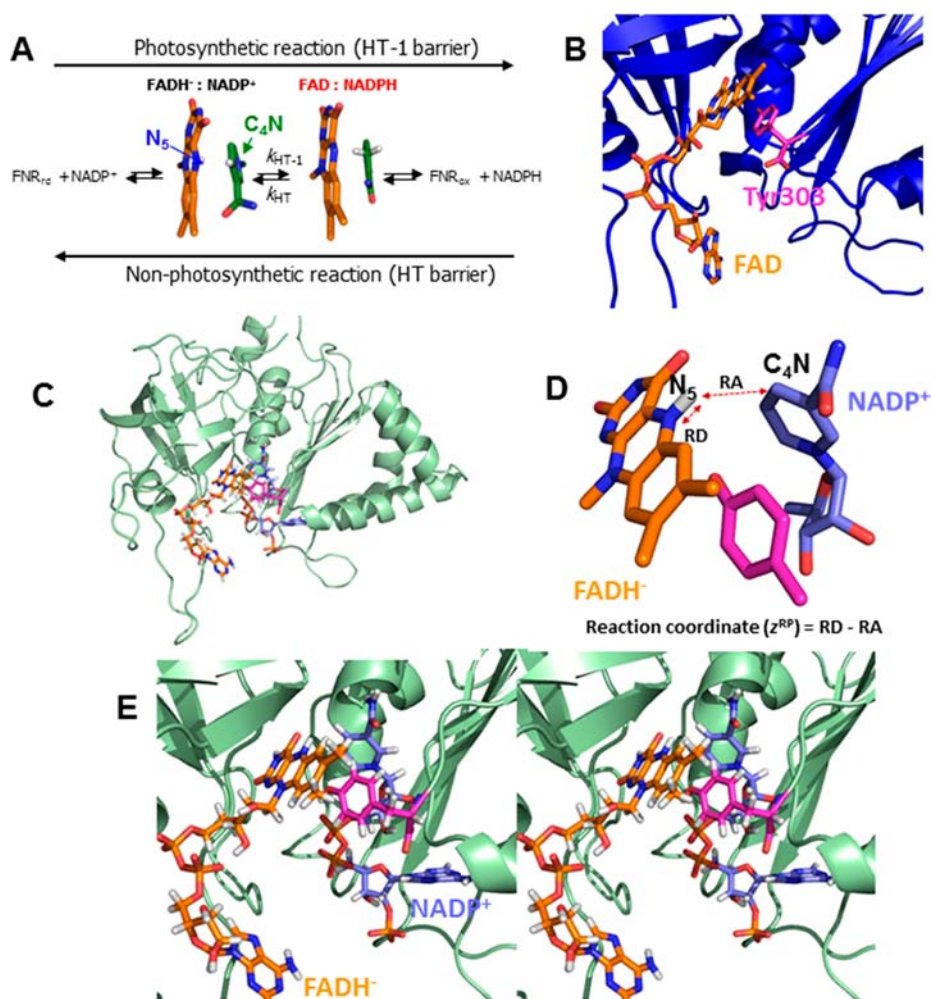


Figure 1. (A) Scheme of the reversible hydride transfer reaction between $\text{FNR}_{\text{rd/ox}}$ and NADP^+/H . (B) Details of the isoalloxazine:Tyr303 stacking found at the active site in the crystal structure of WT *Anabaena* FNR (PDB entry 1que).³ (C) Model of the interaction of WT FNR_{rd} with NADP^+ obtained by MD simulations.²⁰ (D) Geometric definition of the reaction coordinate as the difference between the $\text{N}_5\text{-H}$ and $\text{H-C}_4\text{N}$ distances. (E) Stereoview of the active site in the model obtained by MD, showing a putative catalytically competent architecture for the ternary Tyr303:isoalloxazine:nicotinamide interaction.

maintained by a small two-stranded antiparallel β -sheet at the top. The NADP^+ -binding domain includes residues 139–303 and consists of a core of five parallel β -strands surrounded by seven α -helices.³ The FAD isoalloxazine lies between two tyrosines, Tyr79 and the C-terminal Tyr303, at the interface between the two protein domains. Replacements of Tyr303 by Ser and Glu301 (also situated at the active site) by Ala have been shown to shift the flavin midpoint potential to less negative values, hampering the semiquinone stabilization and introducing barriers to the one-electron transfer processes.^{4,5} Reduction of NADP^+ by FNR_{rd} occurs by a formal hydride transfer from the isoalloxazine anionic hydroquinone to the nicotinamide (Figure 1A). In this process, the protein component of FNR (ApoFNR) has a dual role. On the one hand, it modulates the FAD midpoint potential to a value similar to that of the coenzyme, allowing the hydride transfer to be reversible. Thus, although the main biological function of photosynthetic FNR is the hydride transfer to NADP^+ , the process is reversible *in vivo*. On the other hand, the protein moiety must contribute to facilitating efficient encounter of the reacting atoms, namely, the N_5 of the isoalloxazine, the hydride to be transferred, and the C_4N of the coenzyme.

Over the last 20 years, different biochemical studies have identified the FNR regions involved in determining coenzyme binding, specificity, and enzymatic efficiency.^{6–13} On the basis of several X-ray crystal structures, a stepwise binding mechanism was proposed. The initial step was the recognition of the 2'-P-AMP portion of the coenzyme, which also helps the nicotinamide moiety of NADP^+ to approach a pocket near the FAD cofactor.^{3,14,15} However, in this putative intermediate the C-terminal Tyr of FNR (*AnFNR* Tyr303) stacks against the isoalloxazine ring of FAD, preventing the isoalloxazine:nicotinamide stacking interaction. Therefore, it was expected that an energetically unfavorable displacement of the C-terminal Tyr would be required for the hydride transfer to be possible (Figure 1B). Only FNR variants where the Tyr was replaced provided crystal structures with the nicotinamide and isoalloxazine rings in close proximity, as in the Tyr303Ser FNR: NADP^+ complex.^{8,16} These mutations improved the affinity for NADP^+ and the isoalloxazine:nicotinamide stacking but impaired the physiological hydride transfer to NADP^+ as a result of that strong stacking interaction.^{8,9,16} Recent theoretical quantum mechanics/molecular mechanics (QM/MM) dynamics studies suggested the formation of an [isoalloxazine- H] $^-$: NADP^+ close-contact ionic pair in the reactant complex

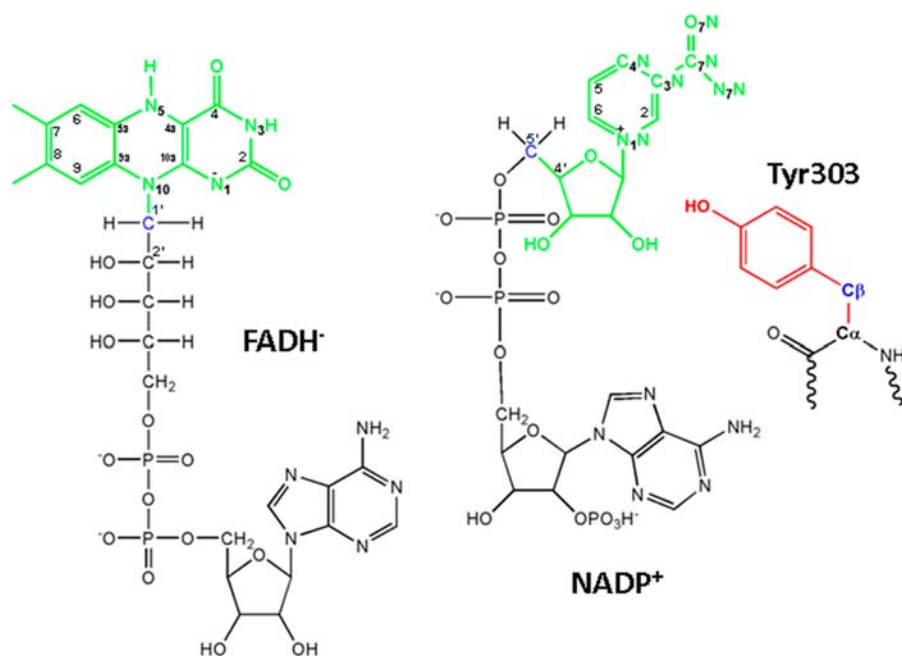


Figure 2. Schematic representation of the molecules that were included in the different QM subsystems (atoms in green and red) used in this work. The boundary atoms are marked in blue.

as the cause of the low reactivity of the mutant in the physiological hydride transfer reaction.¹⁷

In wild-type (WT) FNR, the overall hydride transfer process occurs through a two-step mechanism: initial formation of the $\text{FNR}_{\text{rd}}\text{-NADP}^+$ charge-transfer complex followed by hydride transfer to produce an equilibrium mixture of the $\text{FNR}_{\text{rd}}\text{-NADP}^+$ and $\text{FNR}_{\text{ox}}\text{-NADPH}$ charge-transfer complexes.¹⁸ Both complexes have also been detected for the reverse reaction, despite possible differences in the mechanism.¹⁵ Efficiency in hydride transfer systems involving flavins and pyridine nucleotides usually relies on the approaching distance and collinear orientation of the reacting atoms ($\text{N}_5\text{-hydride-C}_4\text{N}$). Studies of site-directed mutagenesis in the FNR active site indicated that the environment strongly contributes to the relative orientation of the reacting rings, but no strict correlation between the stability of charge-transfer complexes and the rate of the subsequent hydride transfer could be predicted.^{17,19} Therefore, in the WT enzyme, an apparent reduction of the stacking interaction between the isoalloxazine and nicotinamide rings, putatively induced by the C-terminal Tyr side chain, makes the hydride transfer reaction more efficient. Overall, the available data indicate that in WT FNR the C-terminal Tyr prevents the formation of a strong $[\text{isoalloxazine-H}]^-\text{:NADP}^+$ close-contact ionic pair, a fact consistent with the forward (photosynthetic reaction, herein named HT-1) and backward (herein named HT) hydride transfer processes taking place with similar rate constants.

The availability of the structure for the Tyr303Ser *An*FNR complex with NADP^+ allowed some of us¹⁷ to use ensemble-averaged variational transition-state theory with multidimensional tunneling to determine reaction rate constants for the hydride transfer process. The calculated rate constants showed good agreement with the experimental results. These studies additionally provided a description of the structure along the reaction coordinate. A theoretical study of WT FNR was prevented at that time by the lack of reliable structural models representing the transient catalytically competent complexes of

*An*FNR, namely, $\text{FNR}_{\text{ox}}\text{-NADPH}$ and $\text{FNR}_{\text{rd}}\text{-NADP}^+$, particularly the position of the C-terminal Tyr. However, a recent theoretical approach using molecular dynamics (MD) simulations was able to supply putative models for these complexes.²⁰ These models show how the side chain of the C-terminal Tyr303 might contribute to reducing the isoalloxazine:nicotinamide stacking interaction, providing the required spatial disposition of these two rings to permit efficient and reversible hydride transfer (Figure 1C,E).

With the above-mentioned structural models, a theoretical study of the hydride transfer mechanism of WT FNR was carried out. The results obtained are presented in this paper, providing a detailed understanding of how FNR works and shedding light on the contribution of the C-terminal Tyr303 to the architecture of an efficient catalytically competent complex. The comparison with the Tyr303Ser FNR mutant case reveals why the presence of Tyr303 is needed for the photosynthetic hydride transfer to occur.

2. COMPUTATIONAL DETAILS

In the present work, we used the hybrid QM/MM method^{21–24} implemented in CHARMM22²⁵ to describe the hydride transfer reactions between WT *An*FNR $\text{FNR}_{\text{rd}}/\text{FNR}_{\text{ox}}$ and NADP^+/H . Simulations of reactions in large molecular systems, such as protein systems, are possible using the QM/MM methodology, in which the system is partitioned into a QM subsystem, which includes the atoms directly involved in the reaction, and a MM subsystem, which perturbs the QM region through electrostatic and van der Waals interactions. In the dynamic sampling, we employed the semiempirical AM1 method²⁶ to describe the QM region. Although it is well-known that the AM1 method does not take into account the dispersion contribution, which is particularly important in this system, a previous study¹⁷ showed that for this system the AM1 method provides structures in agreement with the crystallographic data. In the subsequent analysis, the semiempirical energies were corrected using the B3LYP functional^{27,28} with the 6-31+G(d,p) basis set and the Grimme dispersion correction (GDC) using the parameters suggested by Grimme for B3LYP (B3LYP-D)²⁹ to account for the $\pi\text{-}\pi$ interactions accurately. The MM subsystem was described using the CHARMM22 force field.

2.1. Molecular Dynamics Equilibration of the Model Structure. The starting structure used to simulate the hydride transfer was a model of the transient catalytically competent WT FNR interacting with its coenzyme, NADP⁺, obtained from a previous study.²⁰ The model structure was solvated with a previously equilibrated cubic box of water molecules centered at the geometric center of the model structure. The initial size of the box was 78 Å × 59 Å × 80 Å. Water molecules within 2.2 Å of any non-hydrogen atom of the protein or ligands were removed. The final model contained 38 663 atoms, of which 4814 were protein atoms. The resultant system was minimized and equilibrated using the AM1/CHARMM22 methodology. The system was partitioned into a QM region consisting of 58 atoms that included the triple ring of the cofactor (FAD/H⁻) and the nicotinamide and ribose rings of the coenzyme (NADP⁺/H). The QM subsystem contained two boundary atoms, the C₁' atom of the flavin ring of FAD/H⁻ and the C₅' atom of the NADP⁺/H (shown in blue in Figure 2), which were represented by the generalized hybrid orbital (GHO) method.²³ The rest of the system was included in the MM region. To remove close contacts and highly repulsive orientations of the initial protein–solvent system, we performed 2500 steps of energy minimization of all solvent molecules using the adapted-basis Newton–Raphson (ABNR) method implemented in the program CHARMM.²⁵ The resultant configuration was heated from 0 to 300 K with protein and coenzyme atoms weakly restrained using a harmonic potential force constant of 20 kcal mol⁻¹ Å⁻². To equilibrate the system, a 250 ps MD simulation was performed with periodic boundary conditions in an isothermal–isobaric (NPT) ensemble at 300 K and 1 atm. A spherical cutoff of 13 Å for the nonbonded interactions was applied together with a switching function acting between 11.5 and 12.5 Å. The nonbonded-pair list was updated every 25 steps. The particle-mesh Ewald method³⁰ with a grid spacing of 1 Å was used for long-range electrostatic interactions. The leapfrog algorithm³¹ was used to propagate the equations of motion with a time step of 2 fs. All bonds involving hydrogen atoms were constrained by the SHAKE algorithm.³²

2.2. Initial 1D Potential Energy Path. From the last structure of the equilibrated ensemble, a one-dimensional (1D) QM/MM potential energy profile for the hydride transfer was calculated along the z^{RP} reaction coordinate, geometrically defined as the difference between the N₅–H distance and the H–C₄N distance (see Figure 1). The QM subsystem included the side chain of Tyr303, the flavin ring of FAD/H⁻, and the nicotinamide and ribose rings of NADP⁺/H. All atoms 20 Å away from the active-site center were kept frozen. The 1D profile was obtained by a series of geometry optimizations of the mobile part of the system (6180 atoms) in the presence of harmonic restraints applied on the reaction coordinate. First, the AM1 method was used to describe the QM region, using the GHO method²³ to represent the QM/MM boundary. Next, the 1D profile was recalculated, including reoptimization, using the B3LYP-D functional for the QM part. In this second case, the standard link atom treatment was used to connect the QM and MM regions. Three link atoms were used (between C₁' and C₂' of FAD/H⁻, between C₄' and C₅' of NADP⁺/H, and between C_α and C_β of the Tyr303 side chain; see Figure 2).

2.3. Reaction Path Refinement Using the Finite-Temperature String Method and Free Energy Calculation along the Reaction Coordinate. We then refined this initial pathway by determining a minimum free energy path between the reactant and product states. To find this reaction pathway, we used an adapted finite-temperature string method^{33,34} combined with the umbrella sampling method to generate different ensembles of configurations along the string. The QM/MM MD calculations used in these string simulations were run with a Langevin thermostat at a temperature of 300 K with 1 fs time step. The total time of the simulation was 855 ps, of which the last 360 ps was used to calculate the minimum free energy path (the first 495 ps was used to optimize the string in the multidimensional space of collective coordinates defined in section 3.2). The standard link atom treatment was used to connect the QM and MM regions as described in section 2.2.

The initial string connecting the reactant and product structures was defined as the curve in the 10-dimensional space of the collective coordinates that connected the 45 images taken from the previously calculated 1D AM1/CHARMM22 potential energy profile. We ran a 1000 fs AM1/CHARMM22 QM/MM MD simulation for each image, saving the trajectory every step, with harmonic restraining potentials centered at each image acting on the collective coordinates. Fitting of high-order polynomial functions over the obtained average collective coordinates along the string was employed to construct an updated string that was again divided into 45 segments. This procedure of carrying out restrained simulations and then updating the string was iterated until the change in the restraint position for the collective coordinates fell below a value of 0.2° for the dihedral angles or 0.01 Å for the distances involved in the set of collective coordinates. Initially, this procedure was iterated 11 times, including 10 distances in the collective reaction coordinate between the donor, acceptor, and hydride atoms involved in the hydride transfer, together with the oxygen and hydrogen atoms of the Tyr303 side chain (more details are given in the Results). From the sampled restrained dynamics data, we evaluated the free energy barrier for the hydride transfer along the reaction coordinate z using a histogram-free implementation of the WHAM equations.^{33,35}

3. RESULTS AND DISCUSSION

3.1. Potential Energy Profiles. We simulated the first step of the hydride transfer process for the photosynthetic generation of NADPH, from FNR_{rd}–NADP⁺ to FNR_{ox}–NADPH, and calculated a 1D QM/MM potential energy profile for the solvated system along the reaction coordinate $z_{\text{AM1}}^{\text{RP}}$, geometrically defined as the difference between the lengths of the breaking N₅–H bond and the forming H–C₄N bond. The potential energy profile was calculated using the AM1 method and the CHARMM22 force field to describe the QM and MM regions, respectively. In the initial calculations, the QM subsystem included the green atoms shown in Figure 2 (see the corresponding results in Figure S1 in the Supporting Information). In subsequent calculations of the potential energy profile, the Tyr303 side chain (red atoms in Figure 2) was also included in the QM region. The structures corresponding to the reactant, transition state (TS), and product were located at $z_{\text{AM1}}^{\text{RP}} = -1.44, -0.24, \text{ and } 1.76$ Å, respectively. In contrast to the results for the potential energy profile previously obtained for the Tyr303Ser FNR mutant model using the same process,¹⁷ here for the WT model we obtained an exoergic reaction (–13.88 kcal/mol). This can be viewed to be the result of destabilization of the reactant, which might be a consequence of the charge separation of the isoalloxazine and nicotinamide rings imposed by the presence of the Tyr303 side chain between them, as on the reactant side the net charges of the isoalloxazine and nicotinamide rings are –1 and +1, respectively. The potential energy difference between the TS and reactant structures (the HT-1 barrier) was 22.35 kcal/mol, whereas the difference between the TS and product structures (the HT barrier) was 36.23 kcal/mol (Figure 3).

The potential energy profile was also calculated for the hydride transfer process along the reaction coordinate $z_{\text{B3LYP}}^{\text{RP}}$, which was defined in the same way as $z_{\text{AM1}}^{\text{RP}}$ but was calculated using the B3LYP-D density functional method with the 6-31+G(d,p) basis set to describe the above-defined QM region, including the Tyr303 side chain. The obtained potential energy profile (Figure 4) also corresponded to an exoergic process (–9.05 kcal/mol), and the potential energy barriers were lower than the ones found using the AM1 method. The potential energy difference between the TS and reactant structures was 14.36 kcal/mol, whereas the difference between the TS and

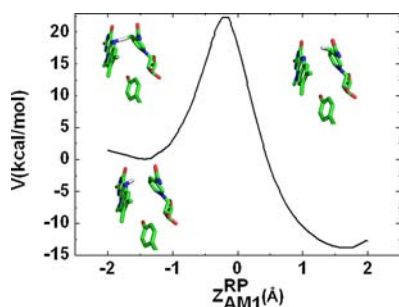


Figure 3. AM1/MM potential energy profile as a function of the z_{AM1}^{RP} reaction coordinate. The relative dispositions of the atoms included in the QM region in the reactant, TS, and product structures are also shown.

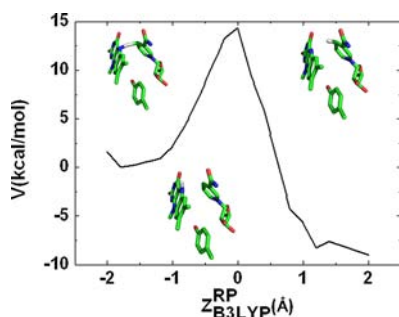


Figure 4. B3LYP-D/MM potential energy profile as a function of z_{B3LYP}^{RP} reaction coordinate. The relative dispositions of the atoms included in the QM region in the reactant, TS, and product structures are also shown.

product structures was 23.41 kcal/mol. Obviously, the lower potential energy barriers obtained with the corrected B3LYP method are, in part, a consequence of taking into account the stabilization due to dispersion interactions. In this particular case, the inclusion of the GDC reduced the reactant–TS potential energy barrier by 1.9 kcal/mol, while the product–TS potential energy barrier was reduced by 4.0 kcal/mol (Figure S2 in the Supporting Information).

3.2. Potential of Mean Force. Initially, the potential of mean force (PMF) along the reaction coordinate z , geometrically defined as the difference between the N_5 –H distance of the breaking bond and the H– C_4N distance of the forming bond, was calculated using the umbrella sampling technique at the AM1/CHARMM22 level. Tyr303 was not included in the QM region, trying to save computational cost. The PMF obtained showed high free energy barriers (33.61 and 41.06 kcal/mol from the reactant and the product, respectively; Figure S3 in the Supporting Information), which do not agree with the experimental rate constants.¹⁷ This fact, together with the experimental evidence that the presence of Tyr303 in the FNR active site might modulate the affinity for the coenzyme⁸ and previous theoretical studies proposing that the Tyr303 side chain might disrupt the ionic pair and π – π stacking interaction between the isoalloxazine and nicotinamide rings,^{17,20} suggested that this residue has an important role in the reaction, both from an electronic point of view and by participating in the nuclear motions that are significant in going from the reactant to the product. Therefore, the Tyr303 side chain had to be included in the QM region and in the set of collective coordinates used to describe the evolution of the reaction. Using the finite-temperature string method, we were able to

incorporate several relevant interatomic distances into the set of collective coordinates (see Computational Details). Thus, to calculate the PMF using the umbrella sampling technique and the string method, we also included distances related to the Tyr303 residue, resulting in the following 10 interatomic distances (Figure 5) defining the set of collective coordinates:

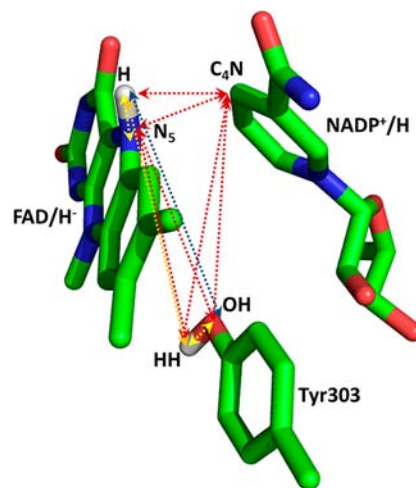


Figure 5. Interatomic distances included as collective coordinates in the definition of the string.

N_5 –H, N_5 – C_4N , N_5 –OH, N_5 –HH, H– C_4N , H–OH, H–HH, C_4N –OH, C_4N –HH, and OH–HH, where N_5 is the donor atom, H the transferred hydrogen, C_4N the acceptor atom, OH the side chain oxygen of Tyr303, and HH the hydrogen bonded to the side chain oxygen of Tyr303.

The string method was initiated with 45 structures obtained from the previously calculated AM1/CHARMM22 potential energy profile (section 3.1). Eleven iterations were performed, and from the sampled restrained dynamics data obtained from these iterations, we evaluated the PMF along the reaction coordinate z using a histogram-free implementation of the WHAM equations^{33,35} (Figure S4 in the Supporting Information).

To analyze whether important coordinates might be missing in the definition of the string, we looked for discontinuities between all possible atom–atom distances within the QM region along the reaction path.³⁶ We found several discontinuities, but all of them were a consequence of a single common effect: the dihedral angle for the amide group of the nicotinamide had different values along the string (Figure S5 in the Supporting Information). We found that the dihedral angle C_4N – C_3N – C_7N – O_7N in the nicotinamide ring could take values of 0° (cis) or 180° (trans) at neighboring windows along the string. Only one of the two conformations was explored in each window, causing the observed discontinuities.

The string method was restarted from the last iteration, this time with the OH–HH distance replaced by the dihedral angle of the amide group of the nicotinamide in the set of collective coordinates. In this way we obtained two different PMFs, the first one with the dihedral angle in the trans conformation and the second one with the dihedral angle in the cis conformation. The PMF with the amide group in the cis conformation showed a lower free energy barrier than the PMF with the amide group in the trans conformation (Figure S6 in the Supporting Information). The PMF with the amide group in the cis conformation was obtained after eight iterations of 1000

fs and is displayed in Figure 6. We computed two PMF curves. The first, $W^{\text{AM1-CM}}(z)$, was obtained by using the semi-

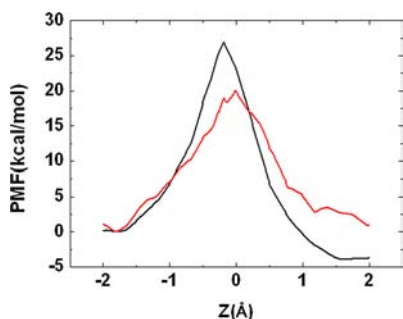


Figure 6. QM/CHARMM22 classical mechanical PMFs with the amide group of the nicotinamide ring in the cis conformation, obtained from string simulations including the dihedral angle of that amide group as one of the collective coordinates. $W^{\text{AM1-CM}}(z)$ (black line) was obtained using AM1 as the QM method in the QM/MM calculation. $W^{\text{DL-CM}}(z)$ (red line) is the dual-level PMF based on the B3LYP-D energy correction.

empirical AM1 method as the QM method of the QM/MM calculations. However, as explained above, the AM1 method fails to describe accurately some interactions, particularly the π - π stacking interactions, which are relevant in the present system. Therefore, a dual-level approach was applied to correct the AM1 energies in a manner similar to that used in previous studies.^{17,37} From the potential energy profiles obtained at the AM1 and B3LYP-D/6-31+G(d,p) levels [$V_{\text{AM1}}(z^{\text{RP}})$ and $V_{\text{B3LYP}}(z^{\text{RP}})$], displayed in Figures 3 and 4, respectively], the dual-level classical mechanical (DL-CM) PMF, $W^{\text{DL-CM}}(z)$, was obtained using the expression

$$W^{\text{DL-CM}}(z) = W^{\text{AM1-CM}}(z) + [V_{\text{B3LYP}}(z_{\text{B3LYP}}^{\text{RP}}) - V_{\text{AM1}}(z_{\text{AM1}}^{\text{RP}})]$$

where the reaction coordinates $z_{\text{B3LYP}}^{\text{RP}}$ and $z_{\text{AM1}}^{\text{RP}}$ emphasize that the correction term (in square brackets) is evaluated along the 1D potential energy reaction paths at the B3LYP-D/CHARMM22 and AM1/CHARMM22 levels.

Figure 6 shows the resulting PMFs. Even though the HT-1 process is also exergonic, the AM1 PMF exhibits several differences in comparison with the AM1 potential energy profile in Figure 3. Importantly, the two free energy barriers, HT-1 (26.91 kcal/mol) and HT (30.84 kcal/mol), are similar. In addition, there is a displacement of the location of the reactant to $z = -1.75$ Å, while the TS and product structures are located at z values close to the ones on the AM1 potential energy profile (i.e., -0.19 and 1.58 Å, respectively). This difference between the AM1 potential energy profile and the corresponding PMF indicates the importance of the entropic contribution to the process.

At this point, the important lowering of the direct and reverse free energy barriers when the finite-temperature string method was employed (compare Figure S3 in the Supporting Information with the black line in Figure 6) merits emphasis. When many geometrical variables can intervene significantly in the definition of the actual reaction coordinate, the string method (combined with umbrella sampling) ensures that the finite sampling of configurations is done in the region around the minimum free energy path. Thus, configurations with greater statistical weight are generated by the calculations along

the string. These configurations can then be binned along the values of a simplified (and convenient) definition of the reaction coordinate, z in this case, leading to a correct PMF as a function of z . Otherwise, if z is directly used to guide the sampling, artificial oscillations of some geometrical variables occur, visiting configurational regions of low probability and leading to a wrong PMF (hysteresis) involving exaggerated free energy barriers. For instance, Figure S7 in the Supporting Information displays different evolutions of the position of Tyr303 depending on how the configurational sampling was carried out. Without the string method, the C-terminal Tyr303, thermally activated and quite free to move, penetrates too much into the region between the isoalloxazine and nicotinamide rings, and only when these two rings approach each other in the TS region is Tyr303 abruptly forced to partially go out of that region. By contrast, the motion of Tyr303 along the string free energy pathway is smooth, as judged by the evolution of the distances in Figure S7.

The introduction of the dual-level correction transformed the process from exergonic to slightly endergonic (Figure 6). The free energy difference between the TS and the reactant in this case was 20.02 kcal/mol, and the difference between the TS and the product was 19.12 kcal/mol. The reactant, TS, and product structures corresponding to $W^{\text{DL-CM}}(z)$ were located at the values $z_{\text{R}}^{\text{DL-CM}} = -1.82$ Å, $z_{\text{‡}}^{\text{DL-CM}} = -0.02$ Å, and $z_{\text{P}}^{\text{DL-CM}} = 1.99$ Å, respectively. The change from exergonic to endergonic was partially caused by the greater stabilization of the reactant compared with the product resulting from the dispersion interactions that were taken into account in the B3LYP-D calculation of the potential energy profile (Figure S2 in the Supporting Information).

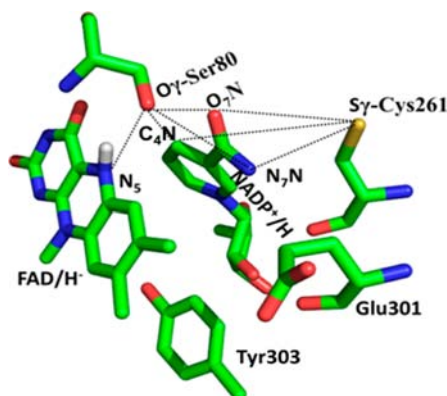
3.3. Role of Tyr303 in the Hydride Transfer Process.

To give insights into the role of the Tyr303 side chain in the active site (whose presence allows WT FNR to catalyze the hydride transfer reaction efficiently in the photosynthetic and backward directions with similar rates), we analyzed how this side chain affects the electrostatic and π - π stacking interactions (by means of the GDC) in the reactant, TS, and product regions.

First, to analyze whether the electric charges of Tyr303 electrostatically stabilize or destabilize the reactant, TS, and product structures, we performed the procedure used by Bash et al.³⁸ We selected all of the configurations obtained along the restrained dynamics simulations with a value of z within ± 0.1 Å of the reactant, TS, or product structure. Next, taking Tyr303 out of the QM region, we performed a single-point energy calculation for each selected structure at the B3LYP-D level using the split valence 6-31+G(d,p) basis set for the QM region. The calculated QM electrostatic energy was then averaged over all of the reactant, TS, and product configurations. These calculations were repeated, but this time the Tyr303 charge was zeroed. The difference between the QM electrostatic energies before and after the charge annihilation provides an estimate of the stabilization/destabilization caused by the charges of the Tyr303 side chain at these stationary structures. The data in Table 1 show that the charges of the Tyr303 side chain very slightly stabilize the reactant respect to the TS and product structures. This result suggests that the electrostatic influence of the side chain of Tyr303 is not relevant for the hydride transfer reaction.

On the other hand, to find out the influence of the π - π stacking interactions on the hydride transfer reaction and how Tyr303 side chain modulates such interactions, we compared

Table 1. Estimation of Electrostatic Stabilization/ Destabilization Caused by the Electric Charges of the Tyr303 Side Chain and the Contribution of the π - π Stacking Interaction Obtained from the GDC for the Reactant, TS, and Product Structures^a



	reactant	TS	product
ΔQM^b	-0.44	-0.37	0.00
GDC Tyr303Ser ^c	-6.51	-8.84	0.00
GDC not Tyr303 ^d	-2.08	-3.75	0.00
GDC WT ^e	-3.76	-5.38	0.00

^aThe energy differences are relative to the product state. All values are in kcal/mol. ^b ΔQM : electrostatic stabilization/destabilization caused by the electric charges of the Tyr303 side chain. ^cGDC Tyr303Ser: estimation of the contribution of the π - π stacking interaction between the isoalloxazine and nicotinamide rings taken into account by the GDC in the mutant Tyr303Ser FNR. ^dGDC not Tyr303: estimation of the contribution of the π - π stacking interaction between the isoalloxazine and nicotinamide rings taken into account by the GDC in WT FNR with the Tyr303 side chain not included in the QM region. ^eGDC WT: estimation of the contribution of the π - π stacking interaction between the isoalloxazine, nicotinamide, and Tyr303 rings taken into account by the GDC in WT FNR.

the GDC average over the reactant, TS, and product structures in both mutant Tyr303Ser FNR (structures taken from Lans et al.¹⁷) and WT FNR (produced in the present study). The results in Table 1 suggest that the dispersion interactions in the mutant mainly stabilize the TS but also that the reactant is stabilized more than the product. Thus, the stabilization due to the dispersion interaction contributes to a significant lowering of the HT barrier and augmentation of the endergonicity, in agreement with the PMF previously obtained for the mutant Tyr303Ser FNR.¹⁷ The values of the GDC for the WT FNR structures with the Tyr303 side chain not included in the QM region also suggest an important stabilization effect due to the

dispersion interaction, again more in the TS than in the reactant. However, this effect is smaller than in the mutant Tyr303Ser FNR. This is an important result because it provides evidence that Tyr303 breaks the π - π stacking interaction between the isoalloxazine and nicotinamide rings. The values calculated for the WT FNR structures from the PMF with Tyr303 included in the QM region and the GDC show an additional stabilizing effect (ca. 1.6 kcal/mol) at both the reactant and the TS due to the dispersion interaction of the side chain of Tyr303 with the isoalloxazine ring and/or the nicotinamide ring. The loss of the dispersion interaction between the isoalloxazine and nicotinamide rings in WT FNR with respect to Tyr303Ser FNR is somewhat higher in the TS than in the reactants. Altogether, these data suggest that the presence of Tyr303 in the active site of WT FNR does not make the HT-1 process easier by decreasing the stabilizing dispersion interactions at the reactant, because the loss of the π - π stacking interaction is even greater in the TS.

We next analyzed how the isoalloxazine and nicotinamide rings geometrically evolve in going from the reactant to the product. The changes in the N_5 - C_4N and N_{10} - N_{1N} distances along the reaction coordinate are shown in Figure 7A. N_{10} and N_{1N} are the atoms opposite N_5 and C_4N in their respective rings, so the difference between these two distances allowed us to envisage the degree of parallelism between the two rings. Those distances were calculated along the reaction coordinate z and averaged over the set of configurations belonging to a given value of the reaction coordinate $z \pm 0.1$ Å. The N_5 - C_4N and N_{10} - N_{1N} distances at the reactant were 3.06 and 6.06 Å, respectively. This result shows that the two rings were more inclined (ca. 66°) against each other in the simulated WT FNR (see Figure S8 in the Supporting Information) than in the crystallographic and simulated structures of Tyr303Ser FNR (ca. 30°), where the average N_5 - C_4N and N_{10} - N_{1N} distances are 3.4 and 4.6 Å, respectively.¹⁷ This difference is due to the presence of Tyr303 in the active site of WT FNR. This residue is not placed between N_5 and C_4N but rather appears in the lower moieties of both rings, separating the two long chains attached to the N_{10} and N_{1N} atoms, respectively. To make the hydride transfer easier, the hydride donor and acceptor atoms have to come closer and the N_5 -hydride- C_4N angle has to approach to 180° (see Figure 7B). These distances evolve similarly as the TS is approached from the reactant side in WT FNR and in the Tyr303Ser FNR mutant.¹⁷ By contrast, the angle between the isoalloxazine and nicotinamide rings (see Figure S8) remains practically invariant from the reactant to the TS (N_5 - C_4N = 2.68 Å and N_{10} - N_{1N} = 5.51 Å) for WT FNR but noticeably increases (N_5 - C_4N = 2.75 Å and N_{10} - N_{1N} =

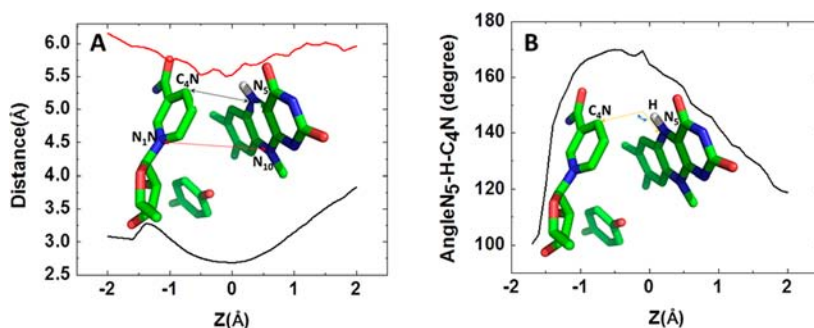


Figure 7. Evolution along the reaction coordinate of (A) the N_5 - C_4N (black) and N_{10} - N_{1N} (red) distances and (B) the N_5 -H- C_4N angle.

4.60 Å) for the Tyr303Ser FNR.¹⁷ The longer distance between the FADH⁻:NADP⁺ ionic pair in WT FNR electrostatically destabilizes the reactant with respect to the situation in Tyr303Ser FNR. This is probably the main kinetic effect of the presence of Tyr303 in the active site of WT FNR and the principal cause of the reduction of the HT-1 classical free energy barrier from 35 kcal/mol in the Tyr303Ser FNR mutant¹⁷ to 20 kcal/mol in the WT FNR, with the corresponding HT free energy barrier remaining practically unchanged.

To highlight the relevance of the loss of electrostatic stabilization in the FADH⁻:NADP⁺ ionic pair in the reactant due to the distortion produced by the presence of Tyr303 in WT FNR, we carried out two different illuminating tests. First, single-point energy calculations at the B3LYP/6-31+G(d,p) level were performed on the atom subsystem marked in green in Figure 2 (H atoms were attached to the N₁₀ and C₄' atoms to saturate their valences) in the reactant and TS structures with geometries extracted from both the WT FNR and Tyr303Ser FNR AM1/MM potential energy profiles (Figure 3 and Figure 6 from Lans et al.,¹⁷ respectively). From these single-point energy calculations, the electrostatic contribution in each structure was obtained by means of a Hirshfeld population analysis^{39–41} including the charge–charge, charge–dipole, and dipole–dipole terms. The results showed that this electrostatic contribution stabilizes the reactant by 5.65 kcal/mol or destabilizes it by 1.26 kcal/mol versus the TS in the Tyr303Ser FNR mutant¹⁷ or the WT FNR, respectively. This simple calculation provided a rough estimate of ca. 7 kcal/mol for the lowering of the barrier of the photosynthetic reaction due to the distortion caused by Tyr303 in WT FNR. On the other hand, as described in section 3.3, from the WT and Tyr303Ser FNR PMFs (Figure 6 and Figure 8 from Lans et al.,¹⁷ respectively) we selected all of the structures belonging to the reactant, and taking nicotinamide, the ribose of NADP⁺, and Tyr303 (in the WT FNR case) out of the QM region, we performed a single-point energy calculation at the B3LYP-D/6-31+G(d,p) level for each selected structure with and without the ribose and nicotinamide MM charges. The difference between the averaged QM electrostatic energies before and after the charge annihilation provided an estimation of the stabilization/destabilization of the reactant caused by the ionic pair for both WT FNR and Tyr303Ser FNR. According to these calculations, that charge annihilation destabilizes the reactant by 7 kcal/mol more in the Tyr303Ser FNR mutant than in the WT FNR.

3.4. Other Residues Forming the Active Site. Several residues of the FNR active-site environment can contribute to the hydride transfer process. Among them are Ser80, Cys261, and Glu301. These residues have been reported to modulate the midpoint reduction potential of the FAD cofactor within the FNR environment as well as the enzyme catalytic efficiency.^{5,10,13,42,43} We analyzed the interactions of these residues with the QM region along the reaction coordinate (Table 2). To do this, we selected all of the configurations obtained along the restrained dynamics simulations with a value of z within ± 0.05 Å of the reactant, TS, and product structures.

The side chain of residue Glu301 pointed its carboxylate group toward the solvent all along the reaction coordinate. This configuration has been previously observed in several X-ray crystal structures as well as in previous theoretical works.^{19,20,44} In those papers, the authors proposed that this residue could be a pathway for proton transfer between the external medium and

Table 2. Calculated Average Distances between the FAD/H⁻ Cofactor or NADP⁺/H coenzyme, and Cys261 or Ser80 in the Reactant, TS, and Product^a

atom 1	atom 2	R \pm 0.05 Å	TS \pm 0.05 Å	P \pm 0.05 Å
S ₇ -Cys261	N ₇ N-NADP ⁺ /H	4.36 \pm 0.01	4.05 \pm 0.02	3.88 \pm 0.01
S ₇ -Cys261	O ₇ N-NADP ⁺ /H	4.86 \pm 0.01	4.35 \pm 0.01	4.56 \pm 0.02
S ₇ -Cys261	C ₄ N-NADP ⁺ /H	6.18 \pm 0.01	6.35 \pm 0.01	5.33 \pm 0.03
O ₇ -Ser80	N ₅ FAD/H ⁻	4.33 \pm 0.01	4.28 \pm 0.01	4.24 \pm 0.02
O ₇ -Ser80	C ₄ N-NADP ⁺ /H	3.65 \pm 0.01	4.15 \pm 0.00	3.83 \pm 0.02
O ₇ -Ser80	O ₇ N-NADP ⁺ /H	2.94 \pm 0.00	2.81 \pm 0.01	2.88 \pm 0.01
O ₇ -Ser80	N ₇ N-NADP ⁺ /H	5.09 \pm 0.00	4.42 \pm 0.02	5.02 \pm 0.01

^aAll values in Å. See the figure in Table 1 for the labeling of the atoms.

N₅ of the flavin via Ser80.⁴⁴ For Cys261, it has been proposed that its side chain pushes the nicotinamide ring toward the isoalloxazine ring by moving its sulfur atom toward the C₄N acceptor atom while this one is receiving the transferring hydride.^{10,13} The sulfur atom of Cys261 approaches the N₇N atom in the amide groups along the reaction path, while the O₇N atom in the same amide group simultaneously hydrogen bonds the hydroxyl group of Ser80. Finally, the hydroxyl group of this residue remains in the environment of the C₄N and N₅ atoms along the reaction coordinate. Therefore, there is a network of interactions between the isoalloxazine and nicotinamide rings, Cys261, and Ser80 that facilitates the approach of the reacting rings, specifically of their N₅H and C₄N atoms. Thus, while Tyr303 separates the lower moieties of the isoalloxazine and nicotinamide rings (the region corresponding to the N₁₀ and N₁N atoms, respectively) and breaks their π – π stacking interactions, the Cys261 and Ser80 residues bring together the upper moieties of these two rings (the region corresponding to the N₅ and C₄N atoms, respectively), contributing to providing the adequate distance and orientation for the chemical step of the reaction event.

4. CONCLUSIONS

In this paper, we have presented a fully microscopic simulation of the hydride transfer processes between *Anabaena* FNR_{rd}/FNR_{ox} and NADP⁺/H with the corresponding solvation shell of water molecules. As the starting structure for our simulations, we used a theoretical structural model recently calculated for the putative transient catalytically competent interaction of *Anabaena* FNR_{rd}/FNR_{ox} with the coenzyme. A dual-level QM/MM hybrid approach was used to describe the potential energy surface of the whole system. MD calculations combining an umbrella-sampling-like implementation of the finite-temperature string method with histogram-free WHAM analysis provided the PMF for the hydride transfer process. The string method has turned out to be essential to ensure sampling of the region of the configurational space that is most relevant for the reactions and avoiding artificial oscillations of some geometrical parameters (as some related to the C-terminal Tyr303). The theoretical results obtained here confirm that the reactant structural model evolves to a catalytically competent transition state through very similar free energy barriers for the photosynthetic (20 kcal/mol) and reverse (19.1 kcal/mol)

reactions, in good agreement with the experimental hydride transfer rate constants reported for this system.

This theoretical approach has additionally provided subtle structural details of the mechanism. In particular, it was of much interest to gain and understanding of why, in spite of the apparent favorable proximity between the isoalloxazine and the nicotinamide rings, the Tyr303Ser FNR mutant does not retain the physiological function that WT FNR has. The intriguing effect of the presence of Tyr303 in the active site of WT FNR is due to the important destabilization (electrostatic + π - π stacking) of the otherwise close-contact ionic pair FADH⁻:NADP⁺ at the reactant. Tyr303 lies between the lower moieties of the isoalloxazine and nicotinamide rings and breaks the π - π stacking interaction between them, in this way contributing to almost complete elimination of the reaction free energy in WT FNR. However, Tyr303 does not make the photosynthetic reaction easier by decreasing the stabilizing dispersion interactions in the reactant because the loss of the π - π stacking interaction is even greater in the TS. On the other hand, the longer distance between the ions in the FADH⁻:NADP⁺ ionic pair in WT FNR electrostatically destabilizes the reactant with respect to the situation in Tyr303Ser FNR. This is probably the main kinetic effect of the presence of Tyr303 in the active site of WT FNR and the principal cause of the reduction of the photosynthetic classical free energy barrier from 35 kcal/mol in the Tyr303Ser FNR mutant¹⁷ to 20 kcal/mol in WT FNR, with the corresponding reverse free energy barrier remaining practically unchanged.

■ ASSOCIATED CONTENT

● Supporting Information

List of abbreviations; complete ref 25b; AM1/MM potential energy profile with the Tyr303 residue not included in the QM region; GDC contribution; PMF with the Tyr303 residue not included in the QM region; PMF obtained from the string simulations including 10 collective coordinates; cis and trans conformations of the amide group; PMF with the amide group of nicotinamide in the trans conformation; evolution of the N₅-O(Tyr303) and C₄N-O(Tyr303) distances; evolution of the angles among the isoalloxazine, nicotinamide, and tyrosine rings; and values of the important geometric parameters in the reactant, TS, and product structures of the AM1/MM and B3LYP-D/MM potential energy profiles. This material is available free of charge via the Internet at <http://pubs.acs.org>.

■ AUTHOR INFORMATION

Corresponding Author

mmedina@unizar.es; mireia@klignon.uab.cat

Notes

The authors declare no competing financial interest.

■ ACKNOWLEDGMENTS

This work was supported by the Ministerio de Ciencia e Innovación, Spain (Grant BIO2010-1493), the Gobierno de Aragón (Grant B18), the Ministerio de Economía y Competitividad, Spain (Grant CTQ2011-24292), and the Generalitat de Catalunya (2009SGR409). I.L. was the recipient of a JAE-CSIC Fellowship associated with the Instituto Química-Física Rocasolano (CSIC).

■ REFERENCES

- (1) Aliverti, A.; Pandini, V.; Pennati, A.; de Rosa, M.; Zanetti, G. *Arch. Biochem. Biophys.* **2008**, *474*, 283–91.
- (2) Medina, M. *FEBS J.* **2009**, *276*, 3942–58.
- (3) Serre, L.; Vellieux, F. M.; Medina, M.; Gómez-Moreno, C.; Fontecilla-Camps, J. C.; Frey, M. *J. Mol. Biol.* **1996**, *263*, 20–39.
- (4) Nogués, I.; Campos, L. A.; Sancho, J.; Gómez-Moreno, C.; Mayhew, S. G.; Medina, M. *Biochemistry* **2004**, *43*, 15111–15121.
- (5) Faro, M.; Gómez-Moreno, C.; Stankovich, M.; Medina, M. *Eur. J. Biochem.* **2002**, *269*, 2656–61.
- (6) Medina, M.; Luquita, A.; Tejero, J.; Hermoso, J.; Mayoral, T.; Sanz-Aparicio, J.; Grever, K.; Gómez-Moreno, C. *J. Biol. Chem.* **2001**, *276*, 11902–12.
- (7) Tejero, J.; Martínez-Júlvez, M.; Mayoral, T.; Luquita, A.; Sanz-Aparicio, J.; Hermoso, J. A.; Hurley, J. K.; Tollin, G.; Gómez-Moreno, C.; Medina, M. *J. Biol. Chem.* **2003**, *278*, 49203–14.
- (8) Tejero, J.; Pérez-Dorado, I.; Maya, C.; Martínez-Júlvez, M.; Sanz-Aparicio, J.; Gómez-Moreno, C.; Hermoso, J. A.; Medina, M. *Biochemistry* **2005**, *44*, 13477–90.
- (9) Piubelli, L.; Aliverti, A.; Arakaki, A. K.; Carrillo, N.; Ceccarelli, E. A.; Karplus, P. A.; Zanetti, G. *J. Biol. Chem.* **2000**, *275*, 10472–6.
- (10) Musumeci, M. A.; Arakaki, A. K.; Rial, D. V.; Catalano-Dupuy, D. L.; Ceccarelli, E. A. *FEBS J.* **2008**, *275*, 1350–66.
- (11) Aliverti, A.; Lubberstedt, T.; Zanetti, G.; Herrmann, R. G.; Curti, B. *J. Biol. Chem.* **1991**, *266*, 17760–3.
- (12) Peregrina, J. R.; Herguedas, B.; Hermoso, J. A.; Martínez-Júlvez, M.; Medina, M. *Biochemistry* **2009**, *48*, 3109–19.
- (13) Sanchez-Azqueta, A.; Musumeci, M. A.; Martínez-Júlvez, M.; Ceccarelli, E. A.; Medina, M. *Biochim. Biophys. Acta* **2012**, *1817*, 1063–71.
- (14) Hermoso, J. A.; Mayoral, T.; Faro, M.; Gómez-Moreno, C.; Sanz-Aparicio, J.; Medina, M. *J. Mol. Biol.* **2002**, *319*, 1133–42.
- (15) Carrillo, N.; Ceccarelli, E. A. *Eur. J. Biochem.* **2003**, *270*, 1900–15.
- (16) Deng, Z.; Aliverti, A.; Zanetti, G.; Arakaki, A. K.; Ottado, J.; Orellano, E. G.; Calcaterra, N. B.; Ceccarelli, E. A.; Carrillo, N.; Karplus, P. A. *Nat. Struct. Biol.* **1999**, *6*, 847–53.
- (17) Lans, I.; Peregrina, J. R.; Medina, M.; Garcia-Viloca, M.; González-Lafont, A.; Lluch, J. M. *J. Phys. Chem. B* **2010**, *114*, 3368–79.
- (18) Tejero, J.; Peregrina, J. R.; Martínez-Júlvez, M.; Gutierrez, A.; Gomez-Moreno, C.; Scrutton, N. S.; Medina, M. *Arch. Biochem. Biophys.* **2007**, *459*, 79–90.
- (19) Peregrina, J. R.; Sanchez-Azqueta, A.; Herguedas, B.; Martínez-Júlvez, M.; Medina, M. *Biochim. Biophys. Acta* **2010**, *1797*, 1638–46.
- (20) Peregrina, J. R.; Lans, I.; Medina, M. *Eur. Biophys. J.* **2012**, *41*, 117–28.
- (21) Warshel, A.; Levitt, M. *J. Mol. Biol.* **1976**, *103*, 227.
- (22) Gao, J. *Rev. Comput. Chem.* **1995**, *7*, 119–85.
- (23) Gao, J.; Amara, P.; Alhambra, C.; Field, M. J. *J. Phys. Chem.* **1998**, *102*, 4714–21.
- (24) Field, M. J.; Bash, P. A.; Karplus, M. *J. Comput. Chem.* **1990**, *11*, 700–33.
- (25) (a) Brooks, B. R.; Bruccoleri, R.; Olafson, B. D.; States, D. J.; Swaminathan, S.; Karplus, M. *J. Comput. Chem.* **1983**, *4*, 187–217. (b) Brooks, B. R.; et al. *J. Comput. Chem.* **2009**, *30*, 1545–614.
- (26) Dewar, M. J. S.; Zoebisch, E. G.; Healy, E. F.; Stewart, J. J. P. *J. Am. Chem. Soc.* **1985**, *107*, 3902–9.
- (27) Lee, C.; Yang, W.; Parr, R. G. *Phys. Rev. B* **1988**, *37*, 785–9.
- (28) Becke, A. D. *J. Chem. Phys.* **1993**, *98*, 5648–52.
- (29) Grimme, S. *J. Comput. Chem.* **2006**, *27*, 1787–99.
- (30) Ulrich, E.; Lalith, P.; Max, L. B.; Tom, D.; Hsing, L.; Lee, G. P. *J. Chem. Phys.* **1995**, *103*, 8577–93.
- (31) Hockney, R. W. *Methods Comput. Phys.* **1970**, *9*, 136–211.
- (32) Ryckaert, J. P.; Ciccotti, G.; Berensden, H. J. *J. Comput. Phys.* **1977**, *23*, 327–41.
- (33) Rosta, E.; Nowotny, M.; Yang, W.; Hummer, G. *J. Am. Chem. Soc.* **2011**, *133*, 8934–41.
- (34) E, W.; Ren, W.; Vanden-Eijnden, E. *J. Phys. Chem. B* **2005**, *109*, 6688–93.

- (35) Kumar, S.; Rosenberg, J. M.; Bouzida, D.; Swendsen, R. H.; Kollman, P. A. *J. Comput. Chem.* **1992**, *13*, 1011–21.
- (36) Rosta, E.; Woodcock, H. L.; Brooks, B. R.; Hummer, G. *J. Comput. Chem.* **2009**, *30*, 1634–41.
- (37) Wong, K.-Y.; Gao, J. *Biochemistry* **2007**, *46*, 13352–69.
- (38) Bash, P. A.; Field, M. J.; Davenport, R. C.; Petsko, G. A.; Ringe, D.; Karplus, M. *Biochemistry* **1991**, *30*, 5826–32.
- (39) Hirshfeld, F. L. *Theor. Chem. Acc.* **1977**, *44*, 129–38.
- (40) Ritchie, J. P. *J. Am. Chem. Soc.* **1985**, *107*, 1829–37.
- (41) Ritchie, J. P.; Bachrach, S. M. *J. Comput. Chem.* **1987**, *8*, 499–509.
- (42) Aliverti, A.; Bruns, C. M.; Pandini, V. E.; Karplus, P. A.; Vanoni, M. A.; Curti, B.; Zanetti, G. *Biochemistry* **1995**, *34*, 8371–9.
- (43) Medina, M.; Martínez-Júlvez, M.; Hurley, J. K.; Tollin, G.; Gómez-Moreno, C. *Biochemistry* **1998**, *37*, 2715–28.
- (44) Dumit, V. I.; Essigke, T.; Cortez, N.; Ullmann, G. M. *J. Mol. Biol.* **2010**, *397*, 814–25.